Geophys. J. Int. (2001) **146,** 619–636

The influence of tectonic plates on mantle convection patterns, temperature and heat flow

Julian P. Lowman,[1,*] Scott D. King[2] and Carl W. Gable[3]

[1] *Institute of Geophysics and Planetary Physics, Los Alamos National Laboratory,* MS C305, *Los Alamos,* NM 87545, *USA*
[2] *Department of Earth and Atmospheric Sciences, Purdue University, West Lafayette,* IN 47907-1397, *USA*
[3] *Geoanalysis* (EES-5), *Los Alamos National Laboratory,* MS F649, *Los Alamos,* NM 87545, *USA*

Accepted 2001 April 3. Received 2001 April 3; in original form 2000 May 31

SUMMARY

The dynamic coupling between plate motion and mantle convection is investigated in a suite of Cartesian models by systematically varying aspect ratios and plate geometries. The aim of the study presented here is to determine to what extent plates affect mantle flow patterns, temperature and surface heat flux. To this end, we compare numerical convection models with free-slip boundary conditions to models that incorporate between one and six plates, where the geometries of the plates remain fixed while the plate velocities evolve dynamically with the flow. We also vary the widths of the plates and the computational domain in order to determine what constraint these parameters place on the mean temperature, heat flux and plate velocity of mantle convection models. We have investigated the influence of plates for three whole-mantle convection cases that differ in their heating modes (internally heated and basally heated) and rheologies (isoviscous and depth-dependent viscosity). We present a systematic investigation of over 30 models that exhibit increasingly complex behaviour in order to understand highly time-dependent systems using the insight gained from simpler models. In models with aspect ratios from 0.5 to 12 we find that for the same heating mode, variations in temperature can be as much as 40 per cent when comparing calculations with unit-width plates to models incorporating plates with widths equal to five times the model depth. Mean surface heat flux may decrease by 60 per cent over the same range of plate widths. We also find that internally heated mantle convection models incorporating plates exhibit novel behaviour that, we believe, has not been described previously in mantle convection studies. Specifically, in internally heated models, plate motion is characterized by episodic reversals in direction driven by changes in the mantle circulation from clockwise to counterclockwise and vice versa. These flow reversals occur in internally heated convection and are caused by a build-up of heat in the interiors of wide convection cells close to mantle downwellings. We find that flow reversals occur rapidly and are present in both single-plate and multiple-plate models that include internal heating. This behaviour offers a possible explanation for why the Pacific plate suddenly changed its direction some 43 Ma.

Key words: convection, dynamics, heat flow, mantle, plate tectonics.

1 INTRODUCTION

Calculations based on boundary layer theory demonstrate that the surface heat flow delivered from a thickening plate decreases rapidly with increasing distance from the diverging plate axis (Turcotte & Oxburgh 1967). This relation between heat flux and plate age suggests that the thermal evolution of the Earth's interior must be profoundly influenced by the geometry of tectonic plates. In comparison with a small plate, less heat per unit area must be lost through a large plate (for this discussion we shall consider a large plate to be a plate that is at least as wide as twice the depth of the mantle), because heat flux is correlated with the age of a plate and large plates incorporate a greater amount of older, thicker, oceanic lithosphere. Mantle convection models that fail to incorporate plates may therefore render inflated estimates of heat loss when compared to models that include at least some large plates.

* Now at: School of Earth Sciences, University of Leeds, Leeds, W. Yorkshire, LS2 9JT, UK. E-mail: j.lowman@earth.leeds.ac.uk

The view of plates as passive rafts carried about on top of the mantle fails to recognize the fact that the stiff upper thermal boundary layer of the convecting mantle's thermally activated rheology (the oceanic lithosphere) defines the plates. Plates are formed from and return to the mantle; accordingly, by referring to the inclusion of plates in convection models we are describing the implementation of a means of encouraging plate-like surface motion to evolve in the model. Incorporating plates in convection models is critical to the study of mantle convection because the Earth is covered by plates and because we know that models that do not include plates evolve differently when compared to models that do include plates.

The influence of plates on convection was studied initially by simulating plate-like surface motions that were obtained by prescribing uniform velocity boundary conditions and fixed plate geometries (e.g. Parmentier & Turcotte 1978; Lux *et al.* 1979; Jarvis & Peltier 1981; Davies 1986, 1988, 1989). Later studies invoked rheological laws or force balance methods to emulate plate-like behaviour, both of which allow the dynamics of the flow to determine plate velocity (e.g. Kopitzke 1979; Davies 1989; Gurnis 1989; King & Hager 1990; Gable *et al.* 1991; Weinstein & Olson 1992; King *et al.* 1992; Monnereau & Quéré 2001). Variations on the latter approach have also allowed for the evolution of plate boundaries (e.g. Zhong & Gurnis 1995a,b; Puster *et al.* 1995; Lowman & Jarvis 1999). In general, the findings of all of these studies indicate that the geometry and motion of the plates influence the wavelength of mantle convection and instill a convective pattern on the mantle's thermal field that reflects the plate dimensions. An important corollary of this result stems from the fact that both surface velocity and convection cell wavelengths impact on surface heat flow and the temperature of a convecting fluid's interior.

In order to study the interactions between large plates and internally heated convection we must investigate a parameter range fitting the Earth. Most importantly we need to study vigorously convecting large aspect ratio models with thermal boundary layers representative of the thickness of the Earth's plates. The importance of studying vigorous, high-Rayleigh-number convection was emphasized by recent results presented by Sotin & Labrosse (1999). These authors showed that for a constant internal heating rate (that is, a constant ratio of internal heating Rayleigh number to Bénard–Rayleigh number), the mean temperature of a convecting fluid decreases as the Bénard–Rayleigh number is increased. Consequently, the thermal contrast between downwellings and the surrounding mantle is increased in high-Rayleigh-number convection. In addition, the velocity fields of internally heated convective flows become progressively more asymmetrical when either the internal heating rate or the Bénard–Rayleigh number is increased (e.g. Jarvis & Peltier 1982). The formation of hot parcels in a convecting fluid's interior is associated with internal heating and is accompanied by asymmetry appearing in the velocity field of the fluid. (That is, downwellings are more focused and faster moving than upwellings.) In higher-Rayleigh-number flows these hot parcels shift towards subduction zones and, due to their buoyancy, create a drag on downwelling flow.

The complexity of the feedback between plate motion and convection is illustrated in this paper by a precursory investigation of 21 models that incorporate single plates that span the width of aspect ratio 0.5, 0.67, 1.0, 2.0, 3.0 and 5.0 calculations. (Reflecting boundary conditions are specified on the sidewalls of these models.) We determine trends in the behaviour of these models when internal heating rates and a depth-dependent mantle rheology are included in the calculations. We then follow our study of single-plate models by investigating a suite of models that incorporate multiple plates in an aspect ratio 12 geometry with periodic (wrap-around) boundary conditions.

We find that, in general, models with plates evolve very differently from free-slip boundary condition models due to the dynamic feedback between the plates and convection. Plate motions in these models adjust dynamically as the flow evolves to reflect the distribution of buoyancy (e.g. Gable *et al.* 1991). Buoyancy-induced stresses drive plates and are responsible for their motion. Convergent plate boundaries determine the locations where mantle downwellings initiate and influence the wavelength (e.g. Gurnis & Zhong 1991) and pattern of convection. Fully dynamic evolution of the models is constrained by the imposition of static plate geometries. (Indeed, a study of similar models incorporating evolving plate boundaries should be the subject of future work.) However, the behaviour of these models exhibits considerable complexity and by restricting the number of intricacies included in the models we have been able to isolate, rather than obscure, the novel physics that results from the feedback between two fundamental features of mantle convection that regulate temperature with different timescales, namely, the presence of plates and internal heating.

Recent advances have been made in developing formulations that allow plate-like behaviour to evolve in mantle convection models without imposed geometrical constraints on the plate geometry, both in 2-D (Richards *et al.* 2001) and in 3-D calculations (e.g. Tackley 1998; Trompert & Hansen 1998). However, these models have not yet been successful in exhibiting long-timescale plate-like behaviour in high-Rayleigh-number calculations. We have implemented an alternative approach to investigating whole-mantle convection over billion-year timescales that makes the study of such problems feasible with existing resources. The models give insight into the effects of plates on mantle convection given the restriction of a non-evolving plate geometry. Although limiting, this restriction allows for a first-order investigation of the interaction between multiple plates with dynamically evolving velocities and high-Rayleigh-number mantle convection.

2 MODEL DESCRIPTION

The failure of infinite Prandtl number convection to exhibit plate-like behaviour when either uniform material properties or temperature-dependent rheologies are specified has been widely described (e.g. Turcotte & Oxburgh 1967, 1972; Richter 1973; McKenzie *et al.* 1974). In general, plate-like surface velocities are obtained in convection models only when a plate generation method is implemented. The plate-like surface motions achieved in these models are obtained by imposing surface velocity as a time-dependent boundary condition (e.g. Gable *et al.* 1991; Lowman & Jarvis 1995, 1996) determined by the dynamics of the convecting system.

We model thick lithospheric plates by specifying a highly viscous layer at the top of the mantle (the model plates) to emulate the high viscosity of the mantle's cold upper thermal boundary layer. Below this layer, we specify either a uniform viscosity or a viscosity that increases with depth. In all cases, the model plates are 1000 times more viscous than the material at their base and extend to a dimensional depth of approximately 145 km (assuming a model depth of 2900 km). Plate

geometries are specified *a priori* and remain fixed for the duration of each model run. The uniform velocity of tectonic plate interiors and the corresponding discontinuities in velocity at plate boundaries are emulated by prescribing surface velocity boundary conditions based on a force balance approach (Gable *et al.* 1991; King *et al.* 1992). This approach for prescribing plate velocities requires the *integrated* shear traction on the base of a plate to vanish at all times. The resulting condition is consistent with a strong rigid plate distributing the applied stresses. By balancing the forces on each plate at each time step, evolving plate motion is obtained that is in dynamic equilibrium with the thermally induced forces driving convection.

We utilize a primitive variables formulation to model infinite Prandtl number Boussinesq convection in a Cartesian geometry. We assume a Newtonian depth-dependent viscosity and allow for the inclusion of uniformly distributed internal heat sources. Accordingly, the non-dimensional mass, momentum and energy conservation laws governing the convective flow take the form

$$\nabla \cdot \mathbf{v} = 0\,, \tag{1}$$

$$\nabla \cdot (\eta(z)\dot{\varepsilon}) - \nabla P = Ra_{\mathrm{B}}\hat{\mathbf{z}} \tag{2}$$

and

$$\frac{\partial T}{\partial t} = \nabla^2 T - \mathbf{v} \cdot \nabla T + \frac{Ra_{\mathrm{H}}}{Ra_{\mathrm{B}}}\,, \tag{3}$$

respectively. The non-dimensional quantities in the above equations are $\mathbf{v}$, the velocity, $\varepsilon(z)$, the depth-dependent dynamic viscosity, $\dot{\varepsilon}$, the strain rate tensor, P, pressure, T, temperature, and t, time. Ra_{B} is the Bénard–Rayleigh number (e.g. Chandrasekhar 1961) and is given by

$$Ra_{\mathrm{B}} = \frac{g\alpha\Delta T d^3}{\kappa v}\,, \tag{4}$$

where g is the gravitational acceleration, α is the thermal expansivity, ΔT is the superadiabatic temperature difference between the top and bottom boundaries, d is the depth of the convecting layer, κ is the thermal diffusivity and v is the kinematic viscosity.

We model convection confined between isothermal horizontal boundaries and include internal heating in a large number of our models. The internal heating rate is specified by the Rayleigh number,

$$Ra_{\mathrm{H}} = Ra_{\mathrm{B}}\,\frac{d^2\varepsilon}{k\Delta T}\,, \tag{5}$$

where k is the thermal conductivity and ε is the rate of internal heat generation per unit volume.

A hybrid spectral finite difference scheme previously described by Gable *et al.* (1991) has been used to solve the system of equations (1)–(3) for 2-D convection. The code has been benchmarked against other numerical models for a variety of problems that do not include plates and shows excellent agreement in those cases (e.g. Travis *et al.* 1991; Busse *et al.* 1993). In addition, the plate model we utilize has been compared with material methods and power law rheology plate generation methods and the agreement between the surface heat flux and plate velocities of these models is excellent (King *et al.* 1992).

3 RESULTS

This study focuses on three types of models: 100 per cent basally heated isoviscous convection (which we have designated Case A), isoviscous convection including internal heat sources (designated Case B) and convection with a depth-dependent viscosity and internal heat sources (Case C). Collectively, we shall refer to Case A, Case B and Case C as the *reference* cases.

In order to make a meaningful comparison of models with different viscosity structures and heating modes we have attempted to match the time-averaged mean surface heat flux from the three reference cases within the limits of the problem. It can be shown that the difference between the mean surface heat flux and the mean basal heat flux, $q_{\mathrm{s}} - q_{\mathrm{b}}$, is equal to the internal heating rate, $Ra_{\mathrm{H}}/Ra_{\mathrm{B}}$, when a steady state is reached in a convecting fluid of unit depth. Consequently, if q_{b} varies, as is the case when an *isothermal* bottom boundary is employed, surface heat flux varies similarly. Nearly all of the models presented in this study are characterized by isothermal boundaries. Accordingly, we specify a Bénard–Rayleigh number as a measure of convective vigour. Since the Earth's plates have a mean thickness of roughly 100–150 km, we have chosen to restrict our study to investigating models with mean upper thermal boundary layer thicknesses in this range. For Bénard convection (Case A) the thermal boundary layers scale to a thickness within the required range when a Rayleigh number (Ra_{B}) of 10^7 is prescribed and the model depth is scaled to the depth of the whole mantle. We have chosen to use the heat flux from a 100 per cent basally heated isoviscous model (Case A) as a reference value. Keeping the ratio of Ra_{H} to Ra_{B} fixed at 15 (discussed below) we made a systematic search of (Ra_{B},Ra_{H}) parameter space and identified a Rayleigh number pair that would give the same heat flux as the Case A model for each of the Cases B and C rheologies. There is an important restriction that accompanies this methodology. Heat flow is affected by convection cell aspect ratio. Thus, if we want to compare models with similar heat fluxes we should match single-cell flow models with the same aspect ratio. The mean temperature and heat flux obtained for Cases A, B and C vary differently for free-slip and no-slip boundary conditions and models that include plates. In addition, the variation is dependent on aspect ratios. Consequently, we are required to match heat fluxes in a model with a specific aspect ratio. We have chosen to match the heat fluxes from the three reference cases in an aspect ratio 3 geometry incorporating a single plate (Table 1, Models A3, B3 and C3). The reasons for this choice are two-fold. First, in all three reference cases a single-cell solution is obtained for this aspect ratio when a viscous plate is specified. Second, the mean plate width in the majority of the multiple-plate models we will study is 3d. Thus, by fixing the heat flux obtained from an aspect ratio 3 model at a specific value, we will be able to test whether heat flow will remain similar in different aspect ratio models when the average plate size in the models is the same. Moreover, if there is a difference, it will be clear whether this is related to the heating mode or to the rheology.

To isolate the effect of internal heating we have examined several additional models that are heated entirely from within. These models are characterized by the same viscosity structure and heating rates as the Case C models; however, the bottom boundary of the models is insulating rather than isothermal. Models with insulating boundaries fundamentally differ from models with isothermal boundaries in that the time-averaged

Table 1. Free-slip surface and single-plate model summary.

Model	Resolution	$\bar{T}$	$\bar{T}$ (2nd moment)	q_s	q_s (2nd moment)	μ	$q_s - q_b$
A1-fs^s	200×200	0.4991	0.00	45.62	0.00	1.00	0.00
B1-fs	200×200	0.6191	0.12×10^{-5}	47.15	0.10×10	1.47	14.98
C1-fs	384×384	0.5902	0.46×10^{-6}	36.42	0.22	1.72	15.25
A12-fs	3888×200	0.4999	0.11×10^{-10}	35.71	0.46×10^{-3}	1.00	0.00
B12-fs	3888×200	0.6242	0.36×10^{-6}	45.30	0.10×10^{-1}	1.49	14.90
C12-fs	4608×400	0.5255	0.41×10^{-11}	33.29	0.19×10^{-3}	1.87	15.49
A.5^s	100×200	0.4625	0.00	49.06	0.00	1.00	0.00
A.67^s	200×200	0.4759	0.00	49.00	0.00	1.00	0.00
A1^s	200×200	0.4903	0.00	46.56	0.00	1.00	0.00
A2	384×200	0.5777	0.29×10^{-7}	29.95	0.30×10^{-1}	1.00	0.00
A3	768×200	0.6391	0.17×10^{-7}	23.38	0.30×10^{-1}	1.00	0.00
A5	1024×200	0.6952	0.25×10^{-8}	20.30	0.30×10^{-2}	1.00	0.00
B.5	100×200	0.6224	0.51×10^{-7}	44.57	0.86×10^{-1}	1.51	14.98
B.67^R	200×200	0.7508	0.20×10^{-5}	37.47	0.51×10	1.63	14.43
B1^R	200×200	0.7983	0.66×10^{-7}	33.34	0.21×10	1.81	14.95
B2^R	384×200	0.9032	0.97×10^{-7}	24.74	0.79	2.52	14.93
B3^R	864×200	0.9468	0.17×10^{-6}	22.04	0.51	3.13	15.00
B5	1296×200	0.9769	0.64×10^{-8}	19.07	0.36×10^{-2}	4.75	15.06
C.5^R	100×200	0.5547	0.39×10^{-5}	40.93	0.18×10	1.58	15.02
C.67^R	200×200	0.6240	0.45×10^{-5}	36.28	0.17×10^{2}	1.72	15.17
C1^R	200×200	0.7008	0.33×10^{-6}	34.48	0.14×10^{2}	1.77	14.99
C2^R	384×200	0.7599	0.20×10^{-4}	28.68	0.20	2.10	15.02
C3	1024×200	0.8374	0.20×10^{-7}	24.71	0.13	2.52	14.92
C5	1024×200	0.8671	0.22×10^{-6}	23.28	0.12×10^{-2}	2.79	14.94

s: steady-state model.
R: Model characterized by flow reversals. Model names indicate the convection mode case (A, B or C) followed by the model aspect ratio (plate width). The designation '-fs' indicates a model with a free-slip upper surface instead of a plate. Case A and Case B convection models are isoviscous. Case C models have a viscosity that increases with depth by a factor of 36. The (Ra_B, Ra_H) values specified for Case A, B and C models are (10^7, 0), (1.5×10^7, 2.25×10^8) and (10^8, 1.5×10^9), respectively. Horizontal × vertical resolution is given in the column headed 'Resolution'. Both vertical and horizontal grid spacing are uniform in all models. Temporally averaged values for global mean temperature, mean surface heat flux, the ratio of surface to basal heat flux and the difference between the surface heat flux and basal heat flux are given for each model in the columns headed $\bar{T}$, q_s, μ and $q_s - q_b$, respectively. Second moment values are also given for $\bar{T}$ and q_s.

mean surface heat flux of such models equals the heating rate, Ra_H/Ra_B, and is therefore a model input parameter and does not vary with parameters such as aspect ratio or plate geometry. However, mean temperature in 100 per cent internally heated models is a function of model geometry and is discussed below.

Average values for the thermal conductivity and the rate of radiogenic heat production in the mantle can be used to obtain a reasonable estimate for the ratio of the internal heating Rayleigh number to the Bénard–Rayleigh number if the superadiabatic temperature across the mantle is known. For whole-mantle convection, Hofmeister (1999) estimated $\Delta T = 2900$ K and thermal conductivity averaged to approximately 4.3 W m^{-1} K^{-1}. Using eq. (5) and taking these values with the depth of the mantle specified as 2900 km, one finds that $Ra_H/Ra_B = 15$ if 4.7×10^{-12} W kg^{-1} is taken as the internal heating rate for the mantle and 4.7×10^3 kg m^{-3} is assumed for the average density of the mantle. This heating rate is roughly in agreement with the estimated heating rates of chondritic meteorites (Stacey 1992).

The depth-dependent viscosity prescribed in Case C is based on the general trend derived from joint inversions of postglacial sea level histories and long-wavelength convectively supported free-air gravity harmonics (Forte & Mitrovica 1996). The viscosity model used is characterized by a factor of 36 increase in viscosity with depth, with the highest gradient occurring in a depth range of 700–1200 km. We use a fit for the radial viscosity profile that was determined by Pysklywec & Mitrovica (1997).

The models in this paper were run for a minimum of 0.2 diffusion time units and in most cases in excess of 0.4 diffusion time units. When scaled to Earth's mantle, this corresponds to a minimum of 100 billion years. It is well known that high-Rayleigh-number, internally heated convection does not achieve a steady-state solution (e.g. Sotin & Labrosse 1999) so we have considered a moving average of several globally calculated quantities to define a 'quasi-steady' state. In the calculations reported in this work there is little variation in the moving average of the plate velocity or surface heat flow time-series (using a time window that is 0.002 diffusion time units in length) even though these time-series vary considerably on timescales much shorter than 0.002 diffusion time units. In general, there are not discernible periodic patterns in these time-series even though the maximum and minimum values in each time-series are well defined. Attempts to characterize the flow behaviour using Poincaré diagrams were therefore generally unsuccessful (some exceptional cases do exhibit clear periodicity). Consequently, we use the time-series of the volume-averaged internal temperature to define a 'quasi-steady' character because it is the last time-series to approach steady behaviour using the 0.002 unit running average window.

3.1 Free-slip surface models

Before analysing any of the models that incorporate plates we shall compare the behaviour of the three reference cases when

free-slip boundary conditions are prescribed. The purpose of examining the free-slip models is to determine the differences that exist in the cases strictly due to varying the heating modes and rheology. We shall also compare the differences that exist between the reference cases when different aspect ratios are prescribed (unit aspect ratio versus aspect ratio 12 models).

In Fig. 1 we present temperature field snapshots from three cases. These models are referred to as Models A1-fs, B1-fs and C1-fs, and correspond to the reference cases A, B and C, respectively, for models where a unit aspect ratio calculation with reflecting sidewalls and free-slip top and bottom boundary conditions are prescribed. In order to maintain a similar degree of vigour in the models we adjust the Rayleigh numbers while adding internal heating and depth-dependent viscosity.

Even at a Rayleigh number of 10^7 it is possible to obtain a steady-state solution for Model A1-fs (Bénard convection) given the boundary conditions stated above. In comparison, Model B1-fs, which includes internal heating ($Ra_H/Ra_B = 15$), is highly time-dependent and oscillates between a convection pattern characterized by either two or four cells. In Model C1-fs, the addition of depth-dependent viscosity re-establishes single-cell flow; however, the flow remains highly time-dependent.

In Table 1 we present the model resolution, and the time-averaged, mean temperature, $\bar{T}$, surface heat flux, q_s, ratio of surface to basal heat flux, μ, and difference in surface and basal heat flux, $q_s - q_b$, for each of the free-slip and single-plate models investigated in this study (isothermal basal boundary conditions only). Also included in the table are second-moment values for $\bar{T}$ and q_s. We calculate the second moments once the models have reached a statistically steady state. The second-moment values are calculated by integrating the values obtained from the square of the difference of the time-series values and their mean. This value is divided by the integral of the mean over the same period. Larger values for a particular second moment indicate that the time-series of the quantity fluctuates from its mean value by a greater amount than a quantity with a smaller second moment.

The table shows that for any given aspect ratio the addition of internal heating increases the mean temperature of the models in calculations both with and without plates. The time-averaged surface heat fluxes obtained from the free-slip isoviscous cases agree fairly closely for the unit aspect ratio model geometry (Models A1-fs and B1-fs); however, the heat flux obtained for Model C1-fs is almost 25 per cent lower than that obtained from Models A1-fs and B1-fs. (The contrast in these heat flux trends differs in the models that include plates and is also a function of model aspect ratio.)

The condition $Ra_H/Ra_B = 15$ implies that all of the internally heated models in this study should yield $q_s - q_b = 15$ once they have reached a state of time-averaged steadiness (that is, a state where the model is neither heating up nor cooling down from its initial condition). In practice, we find that this is not the case. We find that $q_s - q_b$ varies between 14.5 and 15.5 and that the average value can be quite sensitive to the length of the time-averaging window. We also find that some of the models presented show periodic oscillatory behaviour and we find that the average value of Ra_H/Ra_B is much closer to 15 in these cases than in more chaotically time-dependent models. In the latter cases, where periodicity appears absent, time averages may be above or below 15 for unpredictable periods. The values of $q_s - q_b$ included in the tables indicate the average heating rate during the period in which $\bar{T}$ and q_s are calculated.

In Fig. 2 we present temperature field snapshots of Models A12-fs, B12-fs and C12-fs. These three models illustrate examples of Case A, B and C convection, respectively, in aspect ratio 12 boxes with periodic (wrap-around) vertical boundary conditions and free-slip surface boundary conditions. Model A12-fs generally exhibits 12 convection cells of roughly unit aspect ratio but, unlike Model A1-fs, is highly time-dependent. Model B12-fs shows a preference for drifting into a convective pattern arranged into 24 convection cells so that the time-averaged mean cell width in Model B12-fs agrees closely with Model B1-fs. The similarly sized convection cells in Models A1-fs and A12-fs and Models B1-fs and B12-fs result in these pairs of models yielding very similar time-averaged mean temperatures. In contrast, the pattern of convection observed in Model C12-fs differs from Model C1-fs by the greatest wavelength that the box size in Model C12-fs will permit. More specifically, the convective flow in Model C12-fs is time-dependent but remains in a two-cell pattern characterized by a pair of equally sized convection

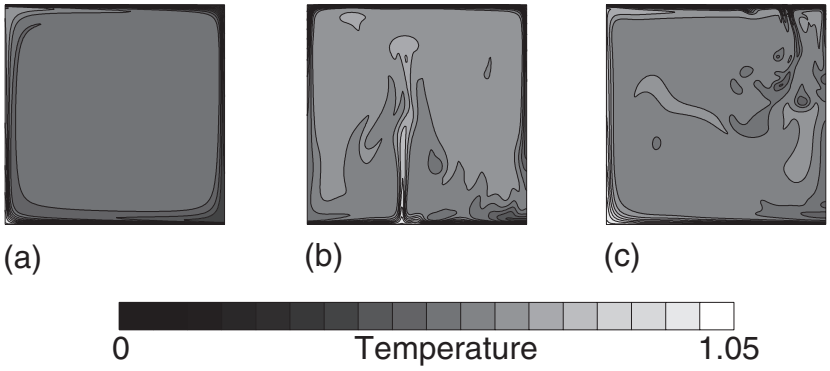

Figure 1. Temperature field snapshots of free-slip boundary convection in unit aspect ratio boxes with reflecting sidewalls. (a) Model A1-fs. Isoviscous basally heated convection with $Ra_B = 10^7$. A steady-state solution is obtained. (b) Model B1-fs. Isoviscous convection with an isothermal bottom boundary and uniformly distributed internal heat sources. $Ra_B = 1.5 \times 10^7$, $Ra_H = 2.25 \times 10^8$. A time-dependent solution is obtained. (c) Model C1-fs. Convection with a depth-dependent viscosity that increases monotonically from top to bottom by a factor of 36. The bottom boundary of the calculation is isothermal, internal heat sources are distributed uniformly. $Ra_B = 10^8$, $Ra_H = 1.5 \times 10^9$. A time-dependent solution is obtained.

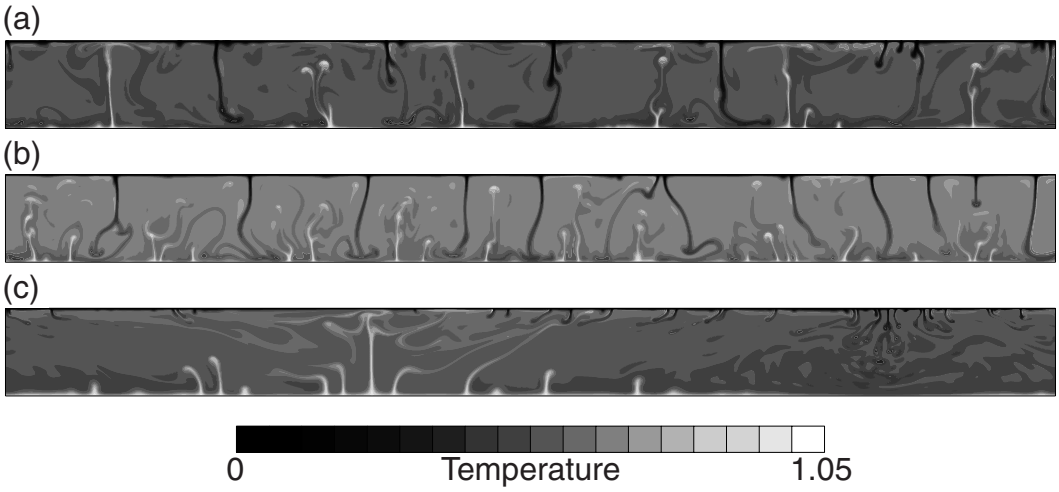

Figure 2. Temperature field snapshots of free-slip boundary convection in aspect ratio 12 boxes with periodic (wrap-around) boundary conditions. All three solutions are time-dependent. (a) Model A12-fs. Isoviscous basally heated convection with $Ra_B = 10^7$. (b) Model B12-fs. Isoviscous convection with an isothermal bottom boundary and uniformly distributed internal heat sources. $Ra_B = 1.5 \times 10^7$, $Ra_H = 2.25 \times 10^8$. (c) Model C12-fs. Convection with a depth-dependent viscosity that increases monotonically from top to bottom by a factor of 36. The bottom boundary of the calculation is isothermal and internal heat sources are distributed uniformly. $Ra_B = 10^8$, $Ra_H = 1.5 \times 10^9$.

cells with aspect ratios of six. Despite the long-wavelength convection characterizing this model, the mean temperature is actually lower in the aspect ratio 12 model than in the aspect ratio 1 model.

The cooling influence of a viscosity that increases with depth has been described in previous mantle convection studies (e.g. Gurnis & Davies 1986). Velocities in the lower thermal boundary layer are retarded by the high viscosity at the base of the box, and the role of advection in the transfer of heat is reduced. In comparison, downwellings are able to form more easily in the less viscous upper thermal boundary layer. The difference in the heat flow at the two boundaries can be viewed in terms of the local Rayleigh numbers of the thermal boundary layers.

The Rayleigh number characterizing the boundary layer is obtained by replacing the layer depth in eq. (4) with the boundary layer thickness. The temperature difference, ΔT, in eq. (4) is replaced with the temperature difference across the boundary layer. The boundary layers become unstable when their thickness becomes great enough that the local Rayleigh number exceeds the critical Rayleigh number (Chandrasekhar 1961; Jarvis & Peltier 1982). Since the viscosity at the bottom of the boxes in Models C1-fs and C12-fs is 36 times greater than that at the top, the lower boundary layer can thicken to 3.3 ($=36^{1/3}$) times the thickness of the top boundary layer before becoming unstable (this argument assumes ΔT across both boundary layers to be the same, which is a useful assumption for understanding the physics of the system, although an approximation). Consequently, the effect of the depth-dependent viscosity is to allow the boundary layer at the base of the box to translate further laterally before becoming unstable than the boundary layer at the top of the box (velocities at the two boundaries will differ so an exact estimate of how much further cannot be obtained). The net result is that short-wavelength instabilities form at the top boundary and cool the depth-dependent viscosity models efficiently and long-wavelength instabilities appear at the bottom boundary and do not heat the models as efficiently as they are cooled.

By decreasing the aspect ratio of a Case C convection model, drips from the upper thermal boundary layer that cool the model interior become less influential (since fewer drips can form in a small box). Thus Model C1-fs is warmer than Model C12-fs.

3.2 Single-plate convection models

Model A1 is a 100 per cent basally heated isoviscous model with one plate. The Bénard–Rayleigh number for this model is 10^7 and, as was the case for Model A1-fs, this model evolves to a steady state. The mean temperature and heat flow calculated from Model A1 (in Table 1) agree with the mean temperature and heat flow from Model A1-fs to within 2 per cent. We suggest that the similarity between the free-slip model and a model incorporating a plate with a width equal to the free-slip convection model cell size verifies that our plate formulation neither drives nor retards the mantle circulation. (Models A1 and A1-fs are the only examples in this study of a pair of models, with and without a plate, of the same case and aspect ratio where the mantle circulation is continually moving in the same direction and the same characteristic convective wavelength is maintained.)

Like Model A1, the two smallest aspect ratio Case A models with plates (aspect ratios 0.5 and 0.67) evolve to steady-state solutions; however, the larger aspect ratio models have developed into single-cell, quasi-steady, time-dependent flows. The presence of the plates in the three widest models (aspect ratios 2, 3 and 5) suppresses instabilities in the upper thermal boundary layers and allows single-cell flow to prevail. In contrast, Case A models with free-slip surfaces develop into multicell flows when aspect ratios of 2, 3 and 5 are specified.

Table 1 shows that as the aspect ratio of these models increases, the mean temperature of the models increases and the average surface heat flux decreases. An increase in temperature with an increase in model aspect ratio was previously observed in models incorporating plates by Lowman & Jarvis

(1996). These authors attributed the temperature increase in wider boxes to the dissimilar nature of the heat transport across the upper and lower boundaries of the models. Their argument is fundamentally the same as the argument given in the previous section to explain why a convecting system with a viscosity that increases with depth is cooler on average than an isoviscous convecting fluid. The suppression of vertical velocity in the viscous plates increases the stability of the upper thermal boundary layer and results in a continued thickening of the boundary layer and reduced heat flow over the width of the model. In contrast, heat flow across the less viscous boundary layer at the bottom of the box is more efficient. Thus, to balance the heat transfer, the mean temperature of the box increases.

3.3 Plates and mantle flow reversals

Table 1 indicates the variability that occurs in heat flow and temperature in different aspect ratio models. A large part of this variability is the result of episodic flow reversals that occur in the internally heated models. We define a flow reversal as a change in the direction of the mantle circulation (e.g. from clockwise to counterclockwise) and a coinciding change in the sign of the plate velocity (in the discussion below, we refer to such events as plate reorganization).

Models characterized by flow reversals are identified in Table 1 by a superscript R. Almost all of the internally heated models in smaller aspect ratio boxes (<3) exhibit frequent flow reversals. The nature of the flow reversals ranges from perfectly periodic to totally unpredictable. In general, we find that increasing the aspect ratios of our models reduces the frequency of the reversals. For example, flow reversals occur in all of the aspect ratio 0.67, 1.0 and 2.0 internally heated models that we have examined; however, flow reversals occur much less frequently in the Case B aspect ratio 3 model and are completely absent in the Case C aspect ratio 3 model. We find the same result when a step function increase in viscosity is specified at a depth of 667 km (assuming a mantle depth of 2900 km) in place of the gradual viscosity increase used in the Case C models. When viscosity is increased by a factor of 30 at 667 km, flow reversals are observed in aspect ratio 1 models but not aspect ratio 3 models. Thus we find that, independent of the gradient of the viscosity increase, a stiff lower mantle acts to stabilize convection patterns in larger aspect ratio models but has little discernible effect on the frequency of flow reversal events in unit aspect ratio models.

Fig. 3 illustrates a sequence of temperature contours from a model that exhibits perfectly periodic flow reversals. This model, B1 in Table 1, differs from Model B1-fs only by the presence of a plate. In Fig. 3(a), counterclockwise motion has been induced by the flushing of the upper thermal boundary layer into the lower mantle at the left-hand side of the figure. The relatively sudden draining of the upper thermal boundary layer entrains a hot parcel of fluid trapped below the viscous plate and drags it into the lower mantle. In Fig. 3(b), the buoyant material entrained by the flushing of the boundary layer starts to ascend as the drag of the cold downwelling wanes. As the hot material rises it begins to push the plate to the right and material in the cold thermal boundary layer flushes into the mantle at the right-hand side of the box (c). In (d), buoyant material has been entrained with the new downwelling; however, the entrained buoyant material again rises

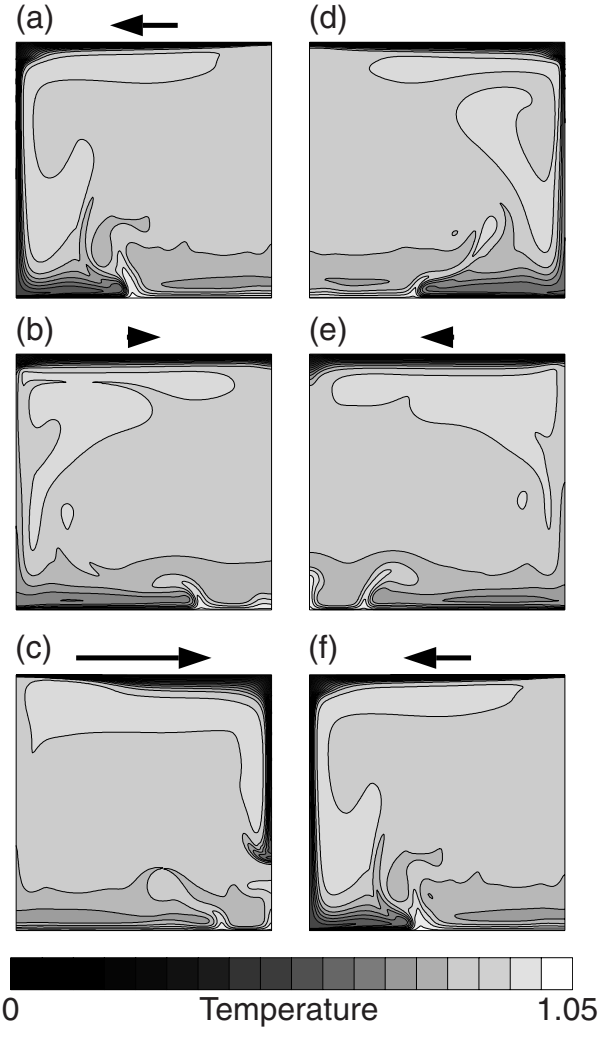

Figure 3. Model B1. Temperature fields from a period covering a single cycle from a model in which flow reverses twice. The model has an aspect ratio of 1.0 and includes uniformly distributed internal heat sources and a plate with a thickness of $0.05d$ (145 km if whole-mantle convection is assumed). The plate has a specified viscosity that is 1000 times more viscous than the isoviscous mantle below. $Ra_B = 1.5 \times 10^7$ and $Ra_B = 2.25 \times 10^8$.

and reverses the flow direction once the intensity of the initial flushing event diminishes (e). In (f) the cycle is about to repeat. The time required to complete the cycle is approximately 300 Myr. This type of behaviour is unique to internally heated models with plates and appears to be driven by the plates trapping internally generated heat in the cores of convection cells that are wider than those found in free-slip boundary condition models.

Fig. 4 shows the surface and basal heat flux obtained from Model B1 (dashed lines) as well as the velocity of the model plate (solid curve). Times corresponding to the panels in Fig. 3 are indicated by vertical lines. The surface heat flux of the model (which is greater than the basal heat flux at all times) surges to a maximum soon after the absolute value of the plate velocity reaches its own maximum. This behaviour corresponds to a high heat flow developing as the upper thermal boundary layer of the model quickly thins, following the change in plate

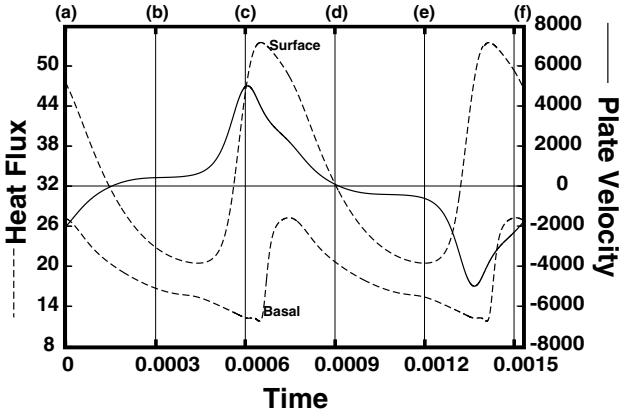

Figure 4. Plate velocity (solid line), surface heat flux and basal heat flux (dashed line) from Model B1 for the period depicted in Fig. 3. Times corresponding to the panels in Fig. 3 are indicated by vertical lines All quantities are non-dimensional.

velocity from almost stationary to rapid. The change in thickness of the thermal boundary layer, which results from the rapid acceleration in plate velocity, can be seen clearly in Fig. 3(c). The maximum basal heat flux occurs as the head of the downwelling spreads out over the base of the box and increases the temperature gradient at the lower boundary (e.g. Fig. 3f).

3.4 Varying heating mode, viscosity stratification and aspect ratio

In Fig. 5 we plot mean temperature as a function of aspect ratio for each of the models included in Table 1. For reference, we plot horizontal lines to indicate the values obtained from the aspect ratio 1 and 12 free-slip calculations. The solid lines correspond to Case A, dashed lines correspond to Case B and dotted lines correspond to Case C. In Cases A and B the mean temperatures from the free-slip unit aspect ratio model are less than that of the aspect ratio 12 model. In contrast, the temperature of the unit aspect ratio model is higher for Case C (as discussed in Section 3.1) and the difference between the temperatures of the two free-slip models is greater than in the other cases. Cases A, B and C models that include a single plate are indicated with circles, triangles and diamonds, respectively. Variations in the values from the time-dependent models are too small to plot but are indicated in Table 1 by the second moment of $\bar{T}$. The temperature increase that occurs with increasing aspect ratio is monotonic in all cases. The data point corresponding to Model A1 (Case A, unit aspect ratio plate) lies almost on top of the solid line that indicates the temperature of the free-slip calculations. With the exception of the models with aspect ratios less than one, all of the internally heated models including plates are hotter than the free-slip models. Thus we find that for any model that has an aspect

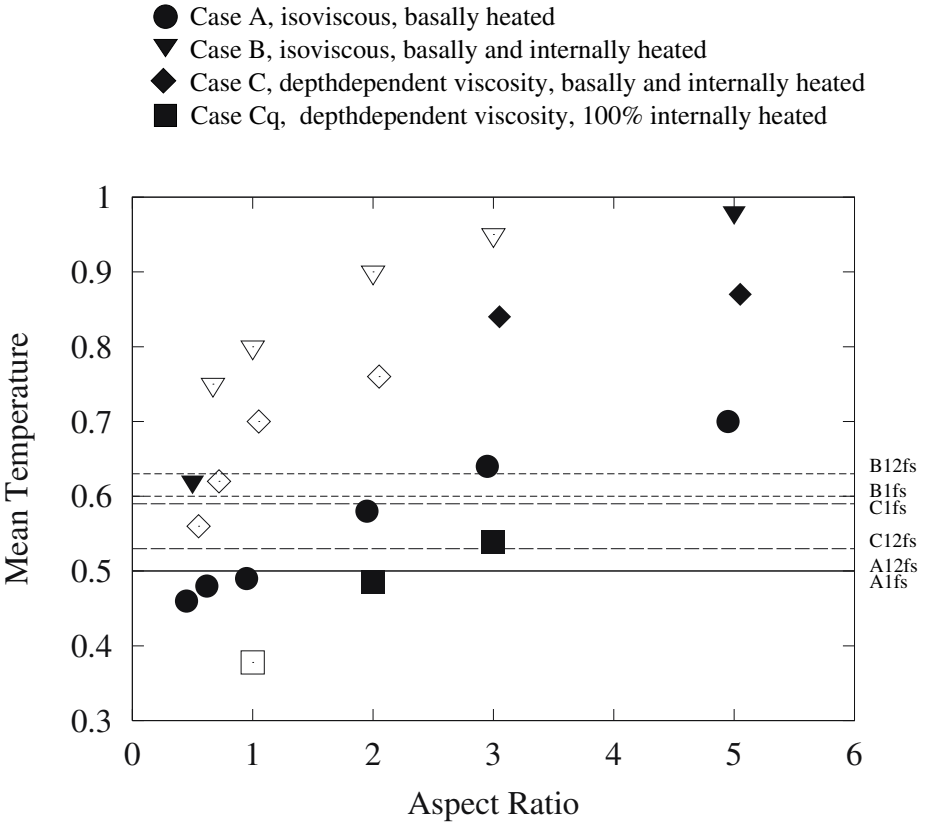

Figure 5. Time-averaged mean temperature as a function of aspect ratio for each of the models in Table 1. Case A, Case B and Case C convection models that include plates are represented with circles, triangles and diamonds, respectively. Case Cq models are represented with squares. Models that exhibit flow reversals (see text for explanation) are represented with open symbols. Reference values from the free-slip models are represented with horizontal lines. The solid line corresponds to Case A models, the long-dashed lines corresponds to Case B models and the short-dashed lines correspond to Case C models. The value from the free-slip aspect ratio 12 model is greater than the value from the free-slip unit ratio model in Cases A and B but not in Case C.

ratio greater than the characteristic wavelength of the cells observed in the free-slip calculations, the inclusion of a plate increases the model temperature.

Fig. 6 shows surface heat flux as a function of aspect ratio for each of the models in Fig. 5 and uses the same symbol convention as Fig. 5. In Fig. 6 we now also use vertical bars to indicate the maximum and minimum values in the time-series from which each data point was determined. We have again used horizontal lines to show reference values from free-slip calculations; however, the maximum values from each free-slip case pair of models now corresponds to the unit aspect ratio models in all three cases. For the purpose of presentation we have clustered the data points around the vertical axis to which they correspond rather than plotting the position of the aspect ratio coordinate precisely. This presentation style allows one to distinguish between the maximum and minimum value bars associated with each point. We find that in all three base cases the mean surface heat flux decreases monotonically as a function of aspect ratio for the models that include a plate. Moreover, the heat flux obtained from the models that have an aspect ratio greater than 1 is less than the heat flux obtained from any of the free-slip calculations. More specifically, the largest plates (aspect ratio 5) retard mantle heat flux by up to 55 per cent in comparison with the heat flux obtained from a unit aspect ratio free-slip calculation.

Fig. 7 shows heat flux ratio as a function of aspect ratio using the same symbol conventions as in Fig. 6. This ratio is a measure of what percentage of the surface heat flux is due to internal heat sources. (For example, if the heat flux ratio is 2 the model is 50 per cent internally heated.) The heat flux ratio in the isoviscous internally heated model increases monotonically and changes by approximately 250 per cent between the aspect ratio 1 and 5 models. Thus 47 per cent of the surface heat flux from the aspect ratio 1 model is due to internal heating but 80 per cent of the surface heat flow from the aspect ratio 5 model is due to internal heat sources. When a free-slip boundary is specified this convection case is approximately 33 per cent internally heated. The increase in the heat flux ratio of the depth-dependent viscosity models is not quite as dramatic but it is still more than 50 per cent. In general, we find that the inclusion of plates in internally heated models can profoundly affect the perceived percentage of the internal heating rate of the model for a fixed rate of internal heating (i.e. fixed Ra_H/Ra_B).

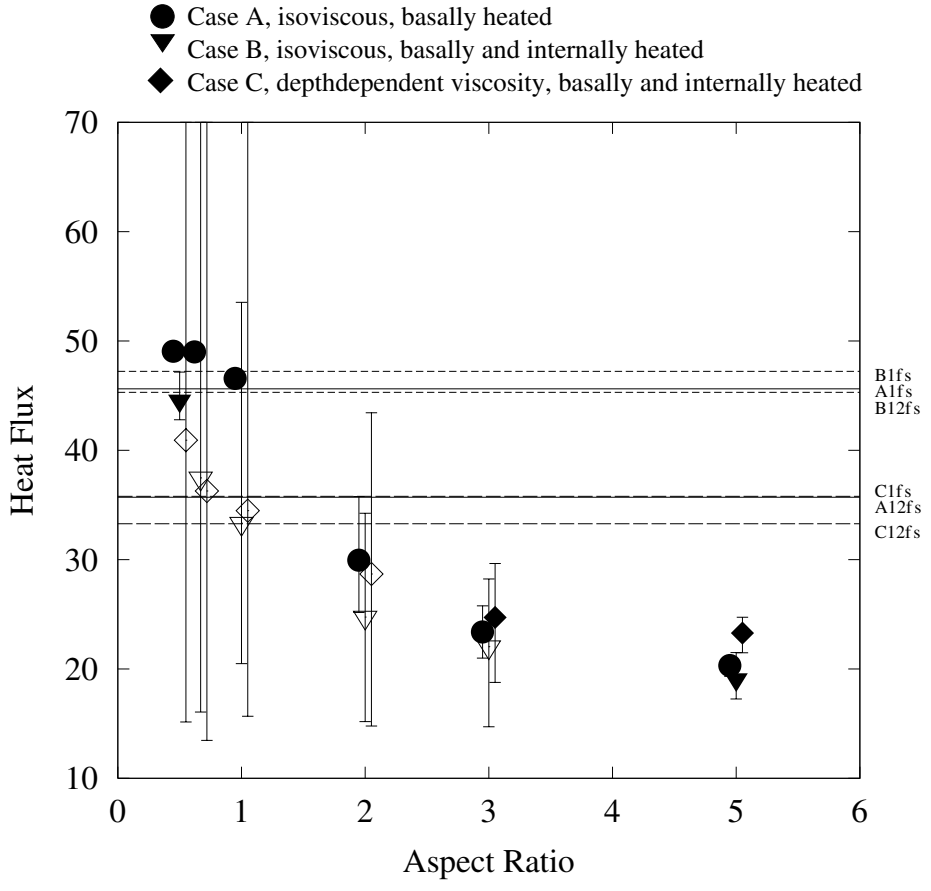

Figure 6. Time-averaged mean surface heat flux as a function of aspect ratio for each of the models in Table 1. Case A, Case B and Case C convection models that include plates are represented with circles, triangles and diamonds, respectively. Maximum and minimum values are indicated with vertical bars. In order to prevent the vertical bars from overlapping we have clustered points around the aspect ratio coordinate to which they correspond. Precise values for the aspect ratios are given in Table 1. Models that exhibit flow reversals (see text for explanation) are represented with open symbols. Reference values from the free-slip models are represented with horizontal lines. The solid lines corresponds to Case A models, the long-dashed lines corresponds to Case B models and the short-dashed lines correspond to Case C models. The value from the unit aspect ratio free-slip model is greater than the value from the aspect ratio 12 model in each case.

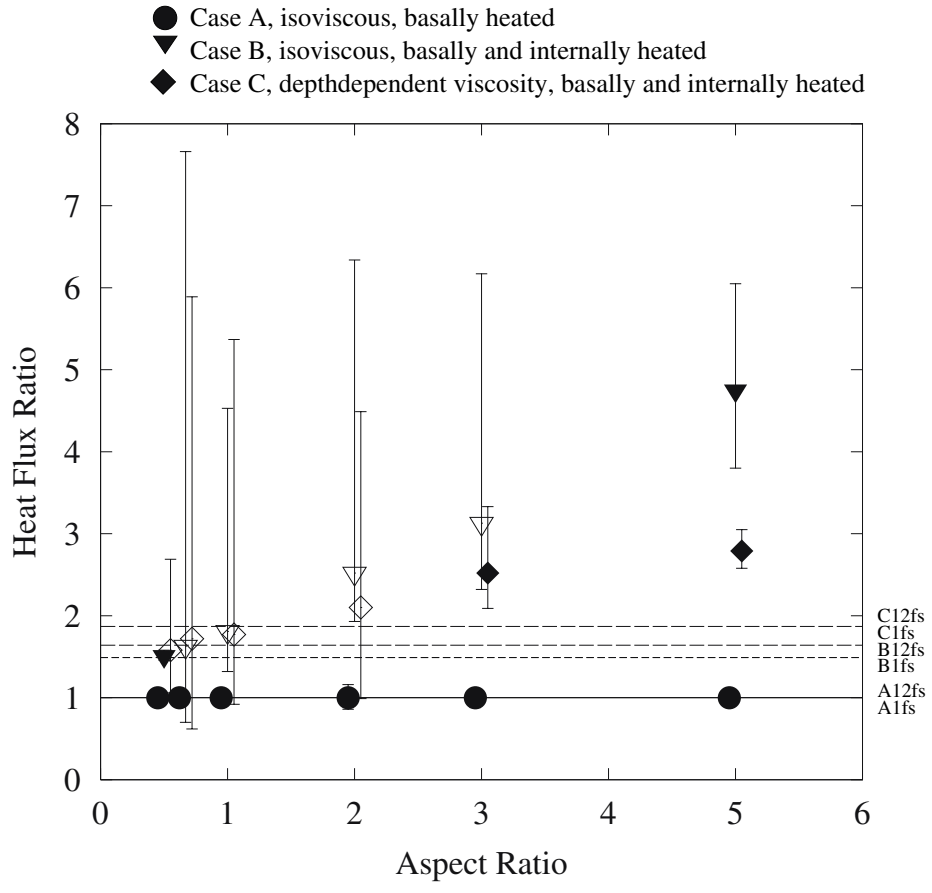

Figure 7. Time-averaged ratio of the mean surface heat flux to the mean basal heat flux as a function of aspect ratio for each of the models in Table 1. Case A, Case B and Case C convection models that include plates are represented with circles, triangles and diamonds, respectively. Maximum and minimum values are indicated with vertical bars. In order to prevent the vertical bars from overlapping we have clustered points around the aspect ratio coordinate to which they correspond. Precise values for the aspect ratios are given in Table 1. Models that exhibit flow reversals (see text for explanation) are represented with open symbols. Reference values from the free-slip models are represented with horizontal lines. The solid lines corresponds to Case A models, the long-dashed lines corresponds to Case B models and the short-dashed lines correspond to Case C models. The values from the free-slip unit aspect ratio and aspect ratio 12 models differ only in Case C. In that case, the aspect ratio 12 model yields a higher value.

The dependence of the ratio of the surface heat flow to the basal heat flow, μ, on model aspect ratio is a fundamental result characteristic of convection with an isothermal bottom boundary condition and internal heating. The presence of plates makes this functional dependence stronger than in models in which plates are absent. Consequently, the percentage of heat flow due to internal heating becomes a function of internal heating rate and model aspect ratio (plate size). Conversely, the mean surface heat flux from a purely internally heated convection model can be prescribed *a priori* and equals the internal heating rate, Ra_H/Ra_B. Instead of heat flux being affected in such models, it is the mean *basal* temperature of the calculations that becomes a strong function of aspect ratio or plate geometry. We have examined three models, C1q, C2q and C3q, that include insulating bottom boundary conditions but which are otherwise identical in all aspects to Models C1, C2 and C3. We find that as was the case for Model C1, flow reversals are frequent and roughly periodic in Model C1q. Similarly, as was the case for Model C3, Model C3q does not exhibit any flow reversals. However, unlike Model C2, Model C2q does not exhibit flow reversals. There are two possible reasons for the difference in the behaviour of the models. One possibility is that in the models with some basal heating (i.e. Model C2) the bottom thermal boundary layer does play some role in inducing flow reversals, perhaps by perturbing the system with the formation of active upwellings. An alternative possibility is that Model C2q, which is constrained to yield a mean heat flux of 15 by the definition of the Rayleigh numbers, is a less vigorous system than Model C2, which produces a heat flux that is almost twice as great (see Table 1). A study of the sensitivity of the flow reversal phenomenon to Rayleigh number should be the topic of a future study.

The resolution and mean temperature, $\bar{T}$, of the single-plate entirely internally heated models is given in Table 2, along with the second moment of the mean temperature. Like the models that include some amount of basal heating, we find that temperature increases as a function of aspect ratio in models that are 100 per cent internally heated. However, the entirely internally heated models are significantly cooler overall (by about 33 per cent). This result is apparently not explained by the fact that the mean surface heat flux from the 100 per cent internally heated models is less than the other models examined. Indeed, if it were true that the mean surface heat flux dictated the mean temperature of these models, then we would expect mean temperatures to converge as aspect ratio is increased in the Case C and Case Cq models (since the heat flux

Table 2. Mean temperatures of entirely internally heated models.

Model	Resolution	$\bar{T}$	$\bar{T}$ (2nd moment)
$C1q^R$	200×200	0.3779	0.25×10^{-7}
C2q	384×200	0.4852	0.11×10^{-7}
C3q	1024×200	0.5395	0.26×10^{-8}

R: model characterized by flow reversals. Model names indicate plate widths. Additional details are given in the text.

from the Case C model starts to approach a value of 15 for larger aspect ratios). However, we do not see evidence of such convergence. Rather, it seems that as aspect ratio is increased, the subducted upper thermal boundary layer material becomes particularly cool (in agreement with travelling a greater distance adjacent to the cooling surface of the model). As a result, the bottom boundary of the 100 per cent internally heated models is dramatically cooled in wide aspect ratio calculations as this cold subducted material spreads out across the base of the models. Consequently, the basal temperature in the models remains low in order to satisfy the insulated bottom boundary condition and the mean temperature of the models remains cooler than in models with basal heating. Additional effects owing to strongly cooled plate material are discussed further in the next section.

3.5 Multiple plate models

We shall continue to consider the three reference case convection models introduced above (Cases A, B and C); however, we now examine the influence of multiple plates in aspect ratio 12 mantle convection models. All of these models have periodic (wrap-around) boundary conditions. Table 3 lists all of the aspect ratio 12 models that we have investigated (excluding the free-slip surface models already included in Table 1) and presents the model resolution, time-averaged, mean temperature, $\bar{T}$, surface heat flux, q_s, ratio of surface to basal heat flux, μ, and difference in surface and basal heat flux, $q_s - q_b$ for each model.

Fig. 8 depicts snapshots of the temperature fields from three basally heated isoviscous convection models (Case A) that include viscous plates with different plate geometries. The models shown in panels a, b and c of Fig. 8 are designated Models A4422, A4242 and A222222 in Table 3. The panels show temperature fields with corresponding instantaneous non-dimensional plate velocities plotted above. (The minimum and maximum values on the vertical axes of the velocity plots are -5000 and 5000.) The Bénard–Rayleigh number of these three models is 10^7 and each model has started from an initial temperature field taken from Model A12-fs.

Model A4422 includes a pair of plates with widths of $4d$ adjacent to a pair of plates with widths of $2d$ (from left to right). From left to right in the figure we shall refer to these plates as plates 1, 2, 3 and 4. After evolving through various flow

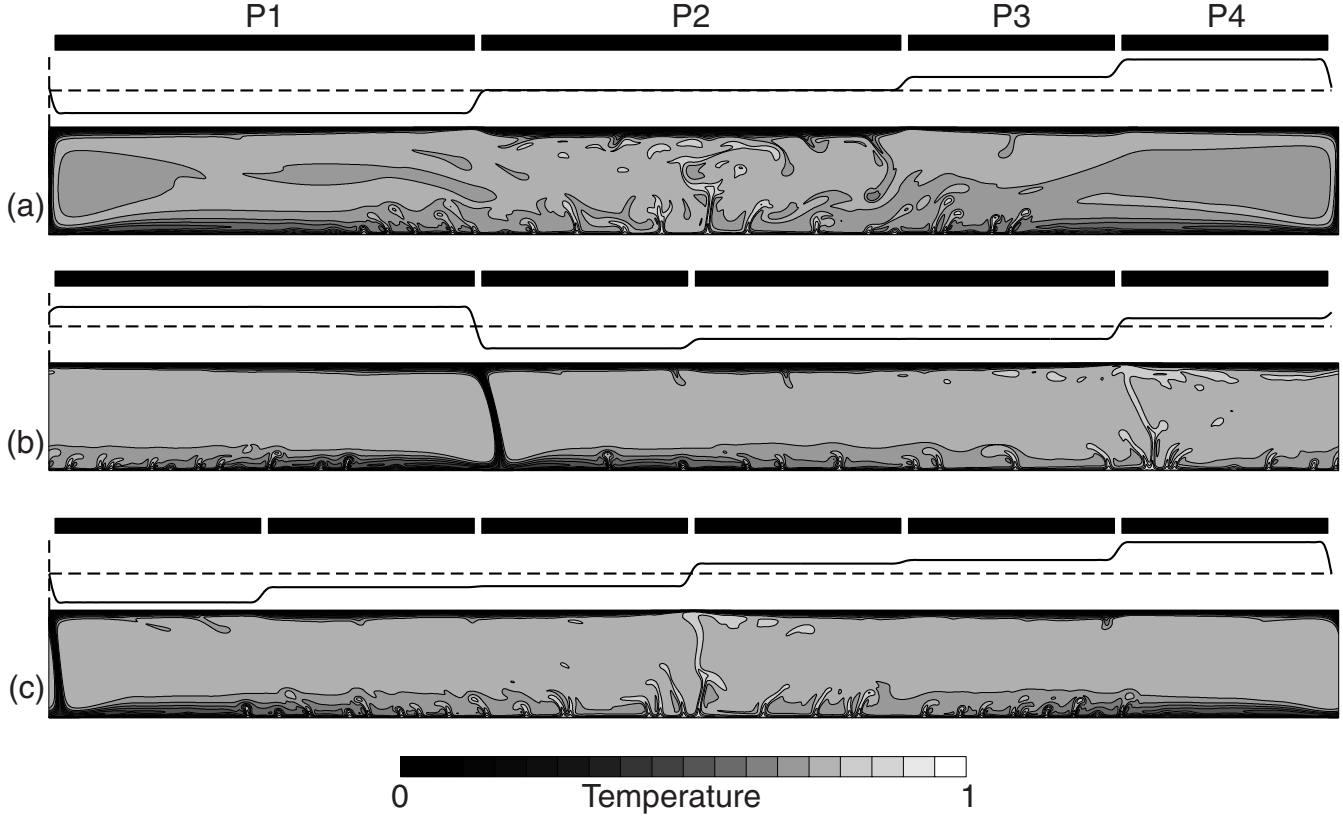

Figure 8. Temperature field snapshots of Models A4422 (a), A4242 (b) and A222222 (c). The instantaneous plate velocities are indicated above each panel in the figure. The range on the velocity axis is from -5000 to 5000 in each case. A non-dimensional velocity of 5000 scales to approximately 5 cm yr^{-1} for whole-mantle convection.

Table 3. Aspect ratio 12; four- and six-plate model summary.

Model	Resolution	$\bar{T}$	$\bar{T}$ (2nd moment)	q_s	q_s (2nd moment)	μ	$q_s - q_b$
A4422	2048×200	0.7139	0.17×10^{-9}	17.39	0.60×10^{-4}	1.00	0.00
A4242	2048×200	0.7328	0.26×10^{-9}	17.78	0.29×10^{-2}	1.00	0.00
A222222	2048×200	0.7266	0.26×10^{-9}	17.89	0.34×10^{-3}	1.00	0.00
B4422	2592×200	0.9427	0.32×10^{-7}	20.19	0.10×10^{-1}	4.17	15.35
B222222	2592×200	0.7266	0.41×10^{-8}	22.42	0.39×10^{-1}	2.90	14.69
C4422	2592×200	0.8681	0.12×10^{-6}	23.65	0.16	2.71	14.92
C4242	2592×200	0.8655	0.55×10^{-8}	23.52	0.50×10^{-2}	2.68	14.74
C222222	2592×200	0.8385	0.10×10^{-6}	25.56	0.59	2.45	15.13
C4422-i	2592×200	0.8452	0.15×10^{-3}	21.46	0.15×10^{-3}	2.94	14.16
C4422q	2592×200	0.6254	0.63×10^{-6}	–	–	–	15.00

Model names indicate the convection mode case (A, B or C) followed by a sequence of digits which each represent the width of one of the plates included in the model. The order of the digits indicates the relative positioning of the plates. The designation '-i' indicates that the model was given a non-random initial condition. (Subduction was intentionally triggered between the two largest plates in this model at the start of the model run.) The designation 'q' indicates a model with an insulating bottom boundary in place of an isothermal boundary. Case A and Case B convection models are isoviscous. Case C models have a viscosity that increases with depth by a factor of 36. The (Ra_B, Ra_H) values specified for Case A, B and C models are (10^7, 0), (1.5×10^7, 2.25×10^8) and (10^8, 1.5×10^9), respectively. Horizontal × vertical resolution is given in the column headed with that title. Both vertical and horizontal grid spacing are uniform in all models. Temporally averaged values for global mean temperatures, mean surface heat flux, the ratio of surface to basal heat flux and the difference between surface heat flux and basal heat flux are given for each model in the columns headed $\bar{T}$, q_s, μ and $q_s - q_b$, respectively. Second moment values are also given for $\bar{T}$ and q_s.

patterns this model locks into the convection pattern shown in Fig. 8(a). A single downwelling is present in the model between plate 1 and plate 4 and a pair of convection cells of approximately aspect ratio 6 have developed with an upwelling centred below plate 2. The surprisingly symmetrical convection pattern results in plate 2 remaining almost motionless and plates 3 and 4 moving in unison towards the mantle downwelling.

Model A4242 includes four plates of widths 4*d*, 2*d*, 4*d* and 2*d* (positioned in Fig. 8b from left to right). The flow in this model again locks into a preferred pattern and again this pattern is dominated by a pair of aspect ratio 6 convection cells (Fig. 8b); however, in contrast to Model A4422, the upwelling flow in Model A4242 is focused below a divergent plate boundary. Model A222222 (Fig. 8c) includes six plates of width 2*d* and evolves into a convection pattern like that reached in Model A4242.

Despite having the apparent freedom to evolve into convection patterns characterized by smaller aspect ratio cells, Models A4422, A4242 and A222222 develop into patterns that have the widest aspect ratio cells that the model size permits. Moreover, although downwellings form at convergent plate boundaries in these models, focused upwellings do not necessarily form where they align with divergent plate boundaries. For example, although the plate geometry specified in Model A4422 would permit the same type of convection pattern to evolve as is observed in Models A4242 and A222222, there is no alignment between the upwelling flow in Model A4422 and a divergent plate boundary. The convection patterns that develop in these models therefore appear to be influenced only by the location of the mantle downwelling and the aspect ratio of the model.

The tendency for the models in Fig. 8 to evolve into a pattern characterized by a single pair of convection cells may result from the vigour of the downwellings that form in these models. The suppression of instabilities in the cool upper thermal boundary layers of these models results in supercool downwellings developing that spread out over the base of the models over distances comparable to the widths of the plates above. Instabilities that form in the lower boundary layer are therefore swept away from the downwelling flow over large distances. In comparison, upwellings draw their source of buoyancy from a limited region of the surrounding thermal boundary layer and therefore contrast less with the temperature of the ambient mantle than downwellings. The stress exerted on the plates by the pull of the downwellings versus the push of the upwellings is illustrated by the surface velocity plots in Fig. 8. Although the six plates included in Model A222222 move similarly to a pair of plates, each plate segment of width 2 moves considerably faster the closer it is to the mantle downwelling.

Figs 9(a), (b) and (c) show the time-series of the velocities of the plates included in Models A4422, A4242 and A222222, respectively. These figures show that in each model an initial period of strongly time-dependent flow characterized by plate flow reversals eventually subsides and is superseded by the development of an organized flow and relatively steady plate velocities. The time required to reach quasi-steady solutions for the models presented in Fig. 8 is considerable and the solutions obtained are dependent on the non-evolving plate geometries. Nevertheless, the presentation of Models A4422, A4242 and A222222 serves to illustrate that high Rayleigh number convection with plates is relatively steady in the absence of internal heating. Moreover, basally heated convection with plates is clearly influenced by model aspect ratio.

In Fig. 10 we present a sequence of 18 temperature fields that illustrate a period in the evolution of an internally heated model with a depth-dependent viscosity (Case C). This model is designated Model C4422 in Table 3 and has exactly the same plate geometry as Model A4422. The flow is highly time-dependent; therefore, in order to capture details in a presentation limited by size, we show the temperature fields from the full aspect ratio 12 model only in the first and last panels of the figure. The middle 16 panels show only the right portion of the solution space depicted in Fig. 10(a). As in Fig. 8, non-dimensional plate velocities are plotted above each panel; however, the minimum and maximum values on the vertical

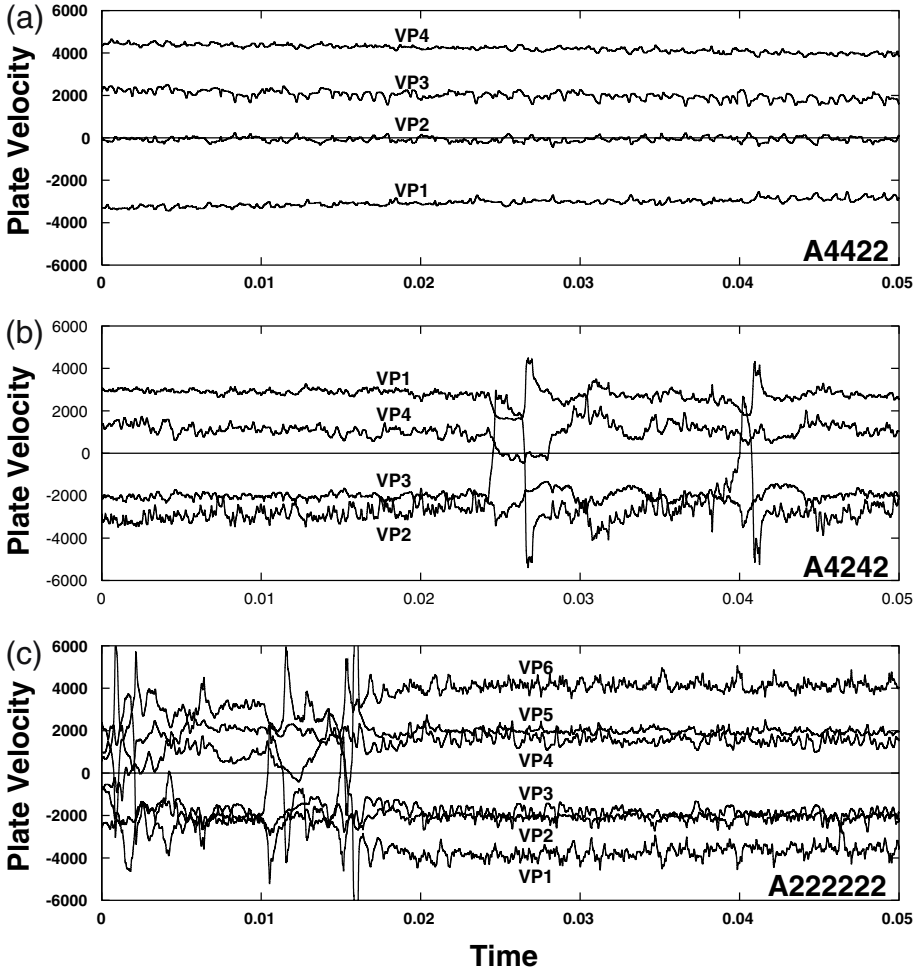

Figure 9. Plate velocity time-series from Models A4422, A4242 and A222222. (a) Velocity as a function of time for each of the plates in Model A4422. (b) Velocity as a function of time for each of the plates in Model A4242. (c) Velocity as a function of time for each of the plates in Model A222222.

axes of the velocity plots are now −8000 and 8000. [Note that in this figure the plate boundaries are not aligned with the ends of the temperature field panels. For example, in Fig. 10(a), all four plate boundaries are located between the ends of the panel and one of the width 4*d* plates spans the panel sidewalls.] At the right of Fig. 10 we plot the time-series of the spatially averaged surface and basal heat fluxes over the period depicted in the panels in Fig. 10 and indicate the times corresponding to the temperature fields depicted in the panels.

The two plates of width 4*d* that are included in Model C4422 move with velocities that vary from nearly stationary to rapid but they do not reverse direction. Indeed, when one of these plates slows the other typically speeds up. Thus, the two large plates almost continually maintain a minimum divergence rate (see Fig. 11, VB12). In contrast, the two plates of width 2*d* reverse their directions regularly.

In Fig. 11 we plot alternating time-series of the velocities of the plates included in Model C4422 (dashed lines) and the rate of convergence of the plates at the plate boundaries (solid lines). The figure is presented with a vertical time axis to convey a sense of plate motion to the left or right in the corresponding frames in Fig. 10. For the time-series of separation rates at the plate boundaries, periods corresponding to plate convergence (i.e. positive values) are shaded. Fig. 11 shows that the flow reversal phenomenon observed in our simple single-plate models is also manifested in larger interconnected systems that incorporate several plates. In addition, the trends observed in the single-plate models seem to carry over to the larger system. Specifically, the smaller (aspect ratio 2) plates in Model C4422 reverse regularly, as was observed in Model C2. In contrast, like the plates in Models C3 and C5, the aspect ratio 4 plates included in Model C4422 do not reverse.

The stability of the pair of large plates in Model C4422 was tested in a model with an identical plate geometry, rheology and heating mode by initiating subduction between the two large plates. We have referred to this test as Model C4422-i in Table 2. This model was allowed to run for a time in excess of 0.05 diffusion times (10 Gyr) and in that time did not exhibit any change in flow pattern from the initial pair of aspect ratio 6 convection cells that had evolved. Thus, we find that a *converging* pair of large plates (identical in size) has an extremely strong stabilizing effect on these models.

Fig. 12 shows a similar plot to Fig. 11 for the time-series data from Model C4242 (a model with alternating width 4*d* and 2*d* plates). In contrast to any of the models presented thus far, we find that plates with widths as great as 4*d* periodically reverse in Model C4242. Consequently, we find that single large plates are less stable (that is, they may reverse) when they are

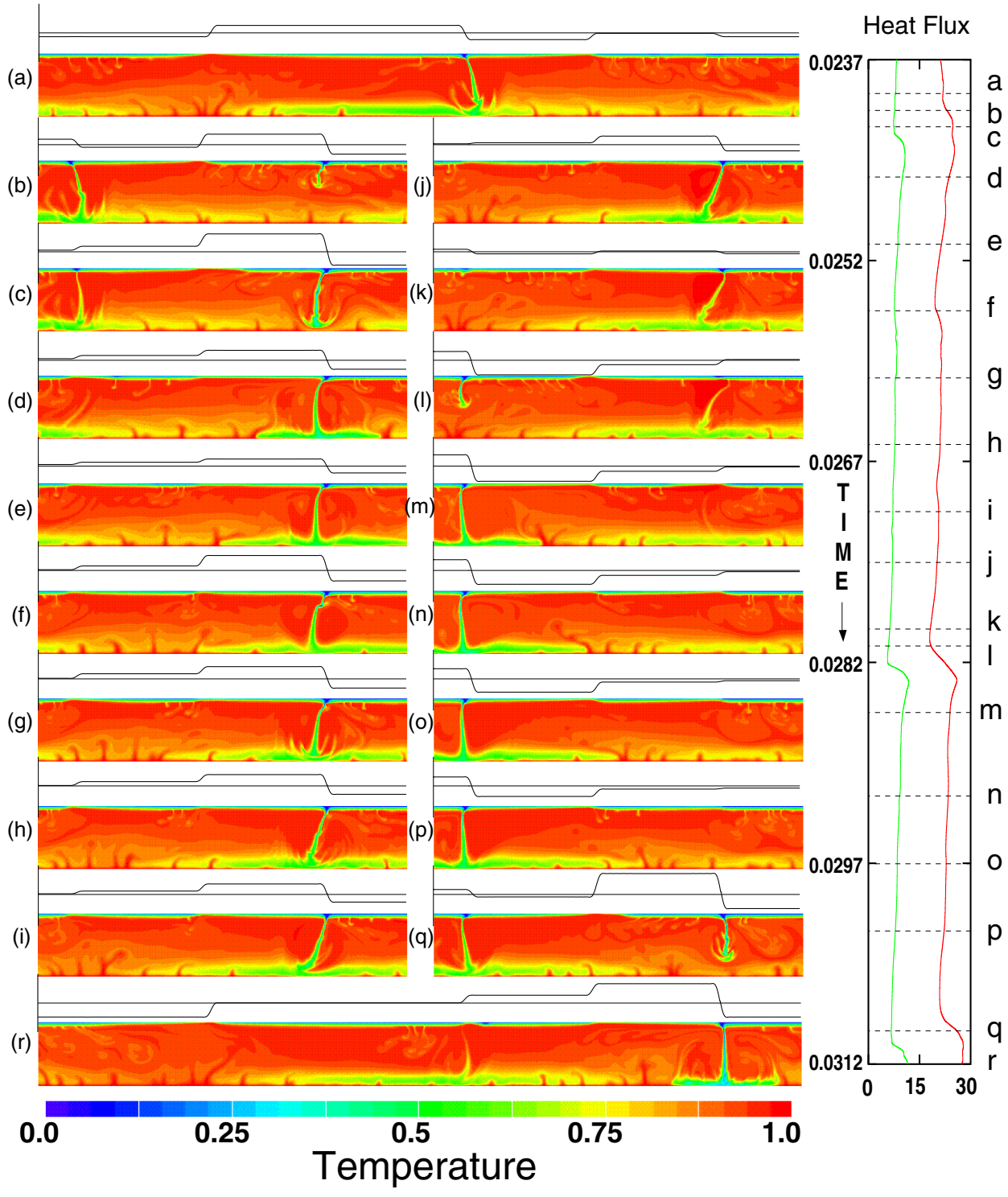

Figure 10. Model C4422. Temperature fields and plate velocity profiles from an aspect ratio 12 model with a depth-dependent viscosity and uniformly distributed internal heat sources. The model has periodic (wrap-around) boundary conditions and incorporates four plates with widths of 4*d*, 4*d*, 2*d* and 2*d*. The Rayleigh numbers specified for the model are $Ra_B = 10^8$ and $Ra_R = 1.5 \times 10^9$. (a) and (r) depict the entire aspect ratio 12 solution domain. (b)–(q) present only the right-hand portion of the solution space shown in (a). Time-series of surface (red) and basal (green) heat flux are shown to the right of the temperature fields and include dashed horizontal lines that indicate the times corresponding to each of the temperature field panels.

located between smaller plates. In all of the previously described internally heated models that did not exhibit flow reversals, the prescribed plate geometries and boundary conditions simulated plates arranged in pairs of equal size. A pair of large plates is apparently more stable than a single large plate.

The most striking feature illustrated in Figs 11 and 12 is that in both models, once convergence (i.e. subduction) initiates at any plate boundary, it fails to endure for more than 0.004 diffusion times (roughly 800 Myr when these models are scaled to whole-mantle convection). Thus, a timescale on the order of

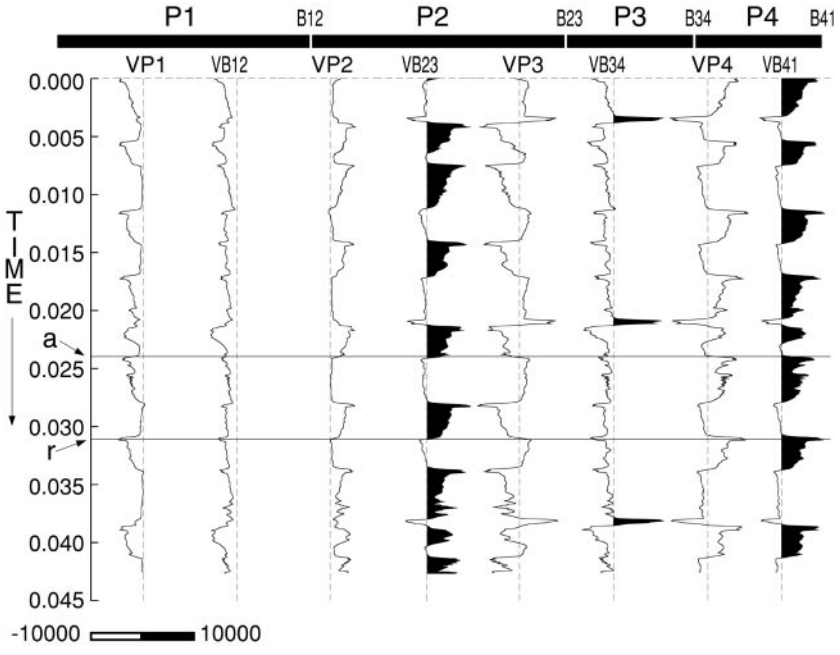

Figure 11. Plate velocity (dashed lines, VP1, VP2, VP3, VP4) and plate boundary convergence velocity (solid lines, VB12, VB23, VB34, VB41) time-series for Model C4422 (Fig. 10). The plate boundary convergence velocity is calculated by taking the difference in the velocity of the plate to the left of the boundary and the velocity of the plate to the right of the boundary. Positive values (shaded) in the plate boundary convergence velocity therefore correspond to convergent plate boundaries and negative values to divergent plate boundaries. Plates 1 and 2 have widths of 4*d*. Plates 3 and 4 have widths of 2*d*.

several hundred million years is long enough, in these models, for a heat build-up to occur that is capable of altering plate velocities by 180° in direction.

The final model examined in the study was an entirely internally heated case with four plates, Model C4422q. We find that, as was the case for Model C4422 (Fig. 10), the model is characterized by frequent reversals of the plates of width 2*d*. The plate boundary between the plates of width 4*d* remains divergent and these plates do not reverse. Qualitatively, this model behaves very much like Model C4422q. However, as was the case in the single plate 100 per cent internally heated models, the mean temperature of Model C4422q was considerably lower than the models with isothermal bottom boundaries (see Table 3).

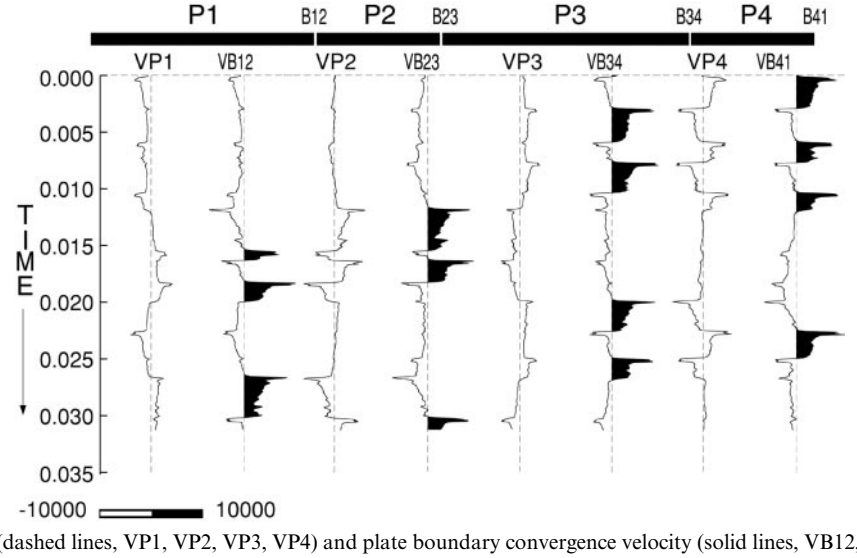

Figure 12. Plate velocity (dashed lines, VP1, VP2, VP3, VP4) and plate boundary convergence velocity (solid lines, VB12, VB23, VB34, VB41) time-series for Model C4242. The plate boundary convergence velocity is calculated by taking the difference in the velocity of the plate to the left of the boundary and the velocity of the plate to the right of the boundary. Positive values (shaded) in the plate boundary convergence velocity therefore correspond to convergent plate boundaries and negative values to divergent plate boundaries. Plates 1 and 3 have widths of 4*d*. Plates 2 and 4 have widths of 2*d*.

4 DISCUSSION AND CONCLUSIONS

The models presented in this paper suggest that by influencing the characteristic wavelength of convection in the mantle, mobile plates profoundly influence the surface heat flux and mean temperature of the mantle.

The response of these systems to large plates can be understood by considering the least complex of the three references cases, Case A (100 per cent basally heated isoviscous convection). In Case A models, a sharp increase in the slope of a log–log plot of mean temperature versus aspect ratio shows that temperature increases more rapidly with the onset of time-dependent flow at an aspect ratio of approximately 1.5. For models with aspect ratios greater than this width, the limit on heat flow from the surface of the system is balanced by the appearance of instabilities in the less stable bottom thermal boundary layer of the models. These instabilities break away from the boundary layer and warm the interior of the convection cells. Consequently, the temperature gradient across the bottom boundary of the system decreases while it increases across the top boundary layer and the mean temperature of the models adjusts to balance the heat flux. The mean temperature of the models therefore increases as plate widths are increased. We find that temperatures in Case A models increase by 40 per cent between a unit aspect ratio and aspect ratio 5 calculation that each incorporate a single plate. In comparison to free-slip convection models, similar temperature increases were also observed in our aspect ratio 12 models that include plates.

We find in all three reference cases that the heat flux from the aspect ratio 12 models that include four plates is lower than it is from the corresponding aspect ratio 3 model that includes a single plate. This is explained most simply by the observation that, in general, longer aspect ratio convection cells form in the aspect ratio 12 models than in the aspect ratio 3 models. Thus model aspect ratio and plate size both affect model temperature, heat flow and convection patterns.

The effect of plates and depth-dependent viscosity both act individually to influence the wavelength of mantle convection. Together, they interact to affect convection cell wavelength in a complex manner. In the absence of plates, wide aspect ratio Case C models are cooler than small aspect ratio Case C models; however, different aspect ratio Case B models without plates are fairly constant in temperature. Thus, the difference in temperature between Case B and Case C models without plates increases with aspect ratio.

In Case C models with plates, the cooling upper thermal boundary layer instabilities that form in wide aspect ratio free-slip boundary condition models are absent. Accordingly, we find that due to the effect of viscosity stratification on convective wavelength, the mean temperature of a Case C aspect ratio 12 multiple-plate convection model can be greater than a similar Case B model. For example, Model B222222 is cooler than Model C222222 because the latter model settles into lengthy periods dominated by long-wavelength convection patterns. The long wavelength is allowed by the large aspect ratio of the model and results from the depth-dependent viscosity. In contrast, Model C2 is considerably cooler than Model B2 because the maximum wavelength of the convection is determined by the calculation aspect ratio to be the same in both models. (Consistent with this finding, we find the surface heat flux from the single-plate models is actually more than in the multiple-plate models in both Cases B and C, thus the freedom to take on different convection patterns does not transfer heat across either of the aspect ratio 12 models more efficiently than implicitly limiting the convection cell size in the aspect ratio 2 models.) When larger plates (width 4 versus 2) are included in the Case B multiple-plate models, the temperature of the models exceeds the similar geometry Case C models because the plates force the Case B model into longer-wavelength convection patterns.

From these findings, we conclude that viscosity structure and aspect ratio both affect model temperatures and that trends in the behaviour of models with plates may be different from models without plates. The effect of model aspect ratio and plate geometry on temperature should therefore receive particular attention when modelling thermally activated rheologies in order to attain plate-like behaviour.

The mean temperatures reported in Table 1 are generally higher than what is expected for the mantle. The Case C models are considered the most Earth-like of the models but when dimensionalized they exhibit temperatures that are probably 20–25 per cent higher than expected for the Earth. Given the input parameters, the two most obvious explanations for this outcome are related to model geometry. Either temperatures may become unrealistically high in 2-D convection models where plates can only move in two directions (which may limit the rate of cooling in the convection model) or Cartesian models with plates and uniform internal heating cannot match the temperatures expected in a spherical shell without some adjustment for differences in geometry. A combination of both of these effects may be reflected in our findings.

The constraint of a 2-D geometry only allows for the plates to change direction by 180°. Numerous examples of such plate reorganizations were observed in this study. However, whether such dramatic changes in plate direction will occur in 3-D models is a subject for future study. In a 3-D geometry, continuous incremental changes in the direction of plate movement may allow for more efficient cooling of the convecting system.

It is also possible that cooler temperatures may exist in the Earth because the ratio of basal to internal heating in a Cartesian geometry results in a different value of μ from that obtained for a spherical shell. The heat flux from the base of the spherical shell mantle must be much higher than that from the base of a plane layer if the basal heat flux is to account for 10–25 per cent of the total surface heat flow, due to the ratio of the inner to outer surface areas of a spherical shell with the dimensions of the whole mantle. Results presented herein show that as the ratio of the surface heat flux to the basal heat flux (i.e. μ) increases, the mean temperature of the convecting system also increases. The effect of large plates on a Cartesian model may therefore inherently escalate the thermal regime to a range that does not agree with constraints on mantle temperatures. Future studies including plates in both 3-D Cartesian and spherical shell geometries will need to be compared with the results presented here in order to settle these issues.

In addition to finding that plates have a significant influence on global thermal quantities, we observed that the feedback between internal heating and plate size has a profound influence on plate velocities. Plates organize significant sources of buoyancy within internally heated models by influencing convective wavelengths. Once formed, these sources of buoyancy grow in intensity and cause rapid changes in plate direction in the highly time-dependent internally heated models presented here. This mechanism for changing plate direction is due to the interaction between two processes with different characteristic

timescales, cooling of the fluid due to plate motion and heating from internal sources. It is the interaction of these two timescales that leads to plate reorganization events. The plate reorganization behaviour manifested in our internally heated models is present in both isoviscous models and models in which viscosity increases with depth. In contrast to the behaviour of internally heated models, we find that 100 per cent basally heated convection is relatively stable and tends to lock into fixed convection patterns for time periods that scale to ages greater than the age of the Earth.

An important restriction placed on the models presented in this work is the non-evolving plate geometries. Indeed, a future suite of calculations will be required in order to test whether the plate reorganization phenomenon observed in these calculations remains a robust feature in models that include evolving plate geometries. (It may also be that evolving plate geometries would allow the models to cool more efficiently.) Numerous examples of flow reversals in the aspect ratio 12 models presented in the previous section indicate that, once formed, convergent plate boundaries fail to endure any longer than about 800 Myr. During a time period of this length it is reasonable to expect that the Earth's plate geometry would completely reorganize, in contrast to the plate geometries in these models. Nevertheless, this study has allowed us to gain an understanding of the feedback between plate motion and internally heated convection by filtering out extraneous complications arising from moving plate geometries.

The limitation of our study to 2-D calculations means that we can only obtain estimates of the time required for changes in plate direction of 180°. Given the freedom of movement in three dimensions, we suggest that buoyant regions trapped below the plates might cause changes in plate direction on the order of tens of degrees on timescales more relevant to evolving plate geometries. Such a phenomenon could explain the rapid change in direction that the Pacific plate underwent approximately 43 Ma.

In our models, the propensity for plates to trap heat in the mantle is illustrated by both the plate reorganization behaviour that arises from a build-up of heat and the rise in mean temperature as larger plates are included in the calculations. In all three of the reference cases examined, the heat flux from the system is reduced as the mean age of the plate increases. Large plates incorporate increasingly greater amounts of the convecting system's older, thicker, upper thermal boundary layer and therefore release less heat per unit area than models with smaller plates. Our results indicate that large plates (whether oceanic or continental) therefore have a profound influence on the thermal structure of the mantle.

ACKNOWLEDGMENTS

We thank P. van Keken, J. Kellogg and G. Ito for helpful comments during the testing of the numerical model. We are grateful to J. Mitrovica and R. Pysklywec for providing the viscosity data implemented in the Case C models. We thank Marc Monnereau and an anonymous referee for helpful reviews. This work was partially supported by the Institute of Geophysics and Planetary Physics and EES Division at Los Alamos National Laboratory. JPL also thanks the Natural Sciences and Engineering Research Council of Canada for financial support. SDK gratefully acknowledges support from the Institute of Geophysics and Planetary Physics at Los Alamos during a sabbatical leave.

REFERENCES

Busse, F.H., *et al.*, 1993. 3D convection at infinite Prandtl number in Cartesian geometry—a benchmark comparison, *Geophys. Astrophys. Fluid Dyn.,* **75,** 39–59.

Chandrasekhar, S., 1961. *Hydrodynamic and Hydromagnetic Stability,* Clarendon Press, Oxford.

Davies, G.F., 1986. Mantle convection under simulated plates: effects of heating modes and ridge and trench migration, and implications for the core–mantle boundary, bathymetry, the geoid and Benioff zones, *Geophys. J. R. astr. Soc.,* **84,** 153–183.

Davies, G.F., 1988. Role of the lithosphere in mantle convection, *J. geophys. Res.,* **93,** 10 451–10 466.

Davies, G.F., 1989. Mantle convection with a dynamic plate: topography, heat flow and gravity anomalies, *Geophys. J.,* **98,** 461–464.

Forte, A.M. & Mitrovica, J.X., 1996. New inferences of mantle viscosity from joint inversion of long-wavelength mantle convection and postglacial rebound data, *Geophys. Res. Lett.,* **23,** 1147–1150.

Gable, C.W., O'Connell, R.J. & Travis, B.J., 1991. Convection in three dimensions with surface plates: generation of toroidal flow, *J. geophys. Res.,* **96,** 8391–8405.

Gurnis, M., 1989. A reassessment of the heat transport by variable viscosity convection with plates and lids, *Geophys. Res. Lett.,* **16,** 179–182.

Gurnis, M. & Davies, G.F., 1986. Numerical study of high Rayleigh number convection in a medium with depth-dependent viscosity, *Geophys. J. R. astr. Soc.,* **85,** 523–541.

Gurnis, M. & Zhong, S., 1991. Generation of long wavelength heterogeneity in the mantle by the dynamic interaction between plates and convection, *Geophys. Res. Lett.,* **18,** 581–584.

Hofmeister, A.M., 1999. Mantle values of thermal conductivity and the geotherm from phonon lifetimes, *Science,* **283,** 1699–1706.

Jarvis, G.T. & Peltier, W.R., 1981. Effects of lithospheric rigidity on ocean floor bathymetry and heat flow, *Geophys. Res. Lett.,* **8,** 857–860.

Jarvis, G.T. & Peltier, W.R., 1982. Mantle convection as a boundary layer phenomenon, *Geophys. J. R. astr. Soc.,* **68,** 385–424.

King, S.D. & Hager, B.H., 1990. The relationship between plate velocity and trench viscosity in Newtonian and power-law subduction calculations, *Geophys. Res. Lett.,* **17,** 2409–2412.

King, S.D., Gable, C.W. & Weinstein, S.A., 1992. Models of convection-driven tectonic plates: a comparison of methods and results, *Geophys. J. Int.,* **109,** 481–487.

Kopitzke, U., 1979. Finite element convection models: comparison of shallow and deep mantle convection and temperatures in the deep mantle, *J. Geophys.,* **46,** 97–121.

Lowman, J.P. & Jarvis, G.T., 1995. Mantle convection models of continental collision and breakup incorporating finite thickness plates, *Phys. Earth planet. Inter.,* **88,** 53–68.

Lowman, J.P. & Jarvis, G.T., 1996. Continental collisions in wide aspect ratio and high Rayleigh number two-dimensional mantle convection models, *J. geophys. Res.,* **101,** 25 485–25 497.

Lowman, J.P. & Jarvis, G.T., 1999. Effects of mantle heat source distribution on supercontinent stability, *J. geophys. Res.,* **104,** 12 733–12 746.

Lux, R.A., Davies, G.F. & Thomas, J.H., 1979. Moving lithosphere plates and mantle convection, *Geophys. J. R. astr. Soc.,* **57,** 209–228.

McKenzie, D.P., Roberts, J.M. & Weiss, N.O., 1974. Convection in the Earth's mantle: towards a numerical simulation, *J. Fluid Mech.,* **62,** 465–538.

Monnereau, M. & Quéré, S., 2001. Spherical shell models of mantle convection with tectonic plates, *Earth planet. Sci. Lett.,* **184,** 575–587.

Parmentier, E.M. & Turcotte, D.L., 1978. Two-dimensional mantle flow beneath a rigid accreting lithosphere, *Phys. Earth planet. Inter.,* **17,** 281–289.

Puster, P., Hager, B.H. & Jordan, T.H., 1995. Mantle convection experiments with evolving plates, *Geophys. Res. Lett.,* **22,** 2223–2226.

Pysklywec, R.N. & Mitrovica, J.X., 1997. Mantle avalanches and the dynamic topography of continents, *Earth planet. Sci. Lett.,* **148,** 447–455.

Richards, M.A., Yang, W.-S., Baumgardner, J.R. & Bunge, H.P., 2001. The role of a low viscosity zone in stabilising plate tectonics: implications for comparative terrestrial planetology G-cubed, in press.

Richter, F.M., 1973. Dynamical models for sea floor spreading, *Rev. Geophys. Space Phys.,* **11,** 223–287.

Sotin, C. & Labrosse, S., 1999. Three-dimensional thermal convection in an iso-viscous, infinite Prandtl number fluid heated from within and from below: applications to the transfer of heat through planetary mantles, *Phys. Earth planet. Inter.,* **112,** 171–190.

Stacey, F.D., 1992. *Physics of the Earth,* 3rd edn, Brookfield Press, Brisbane.

Tackley, P.J., 1998. Self-consistent generation of tectonic plates in three-dimensional mantle convection, *Earth planet. Sci. Lett.,* **157,** 9–22.

Travis, B., *et al.*, 1991. A benchmark comparison of numerical methods for infinite Prandtl number thermal convection in two-dimensional Cartesian geometry, *Geophys. Astrophys. Fluid. Dyn.,* **55,** 137–160.

Trompert, R. & Hansen, U., 1998. Mantle convection simulations with rheologies that generate plate-like behaviour, *Nature,* **395,** 686–689.

Turcotte, D.L. & Oxburgh, E.R., 1967. Finite amplitude convection cells and continental drift, *J. Fluid Mech.,* **28,** 29–42.

Turcotte, D.L. & Oxburgh, E.R., 1972. Mantle convection and the new global tectonics, *Ann. Rev. Fluid Mech.,* **4,** 33–68.

Weinstein, S.A. & Olson, P.L., 1992. Thermal convection with non-Newtonian plates, *Geophys J. Int.,* **111,** 515–530.

Zhong, S. & Gurnis, M., 1995a. Towards a realistic simulation of plate margins in mantle convection, *Geophys. Res. Lett.,* **22,** 981–984.

Zhong, S. & Gurnis, M., 1995b. Mantle convection with plates and mobile, faulted plate margins, *Science,* **267,** 838–843.